Investigation of the frozen-turbulence hypothesis for temperature spectra in a convectively mixed layer

J. W. Deardorff and G. E. Willis

Citation: Physics of Fluids **25**, 21 (1982); doi: 10.1063/1.863623
View online: http://dx.doi.org/10.1063/1.863623
View Table of Contents: http://scitation.aip.org/content/aip/journal/pof1/25/1?ver=pdfcov
Published by the AIP Publishing

Investigation of the frozen-turbulence hypothesis for temperature spectra in a convectively mixed layer

J. W. Deardorff and G. E. Willis

Department of Atmospheric Sciences, Oregon State University, Corvallis, Oregon 97331
(Received 29 April 1981; accepted 23 October 1981)

Taylor's frozen turbulence hypothesis is investigated in a laboratory free-convection mixed layer which can simulate buoyancy-driven turbulence in an atmospheric mixed layer (of height h) for mean wind speeds of up to several meters per second. For large turbulence intensities the temperature spectra at the height $0.1h$ are found to be spuriously enhanced at higher wavenumbers based on the frozen turbulence hypothesis, as deduced theoretically by previous investigators. The excess is borrowed from spectral intensities within the energy-containing range. A theory based on the concept of longitudinal-temporal isotropy, after proper scaling of the coordinates, is shown to predict a simple shift of the entire spectrum toward higher wavenumbers with increasing turbulence intensity. The failure of the observed spectra to behave this simply is associated with a complicated structure of the correlation coefficient as a function of longitudinal-temporal lag coordinates when the former is measured relative to a frame moving with the mean flow speed. The temperature spectrum based on the frozen-turbulence hypothesis appears to be a satisfactory representation of the true spectrum in wavenumber space, in tubulence dominated by thermal convection, if the mean wind speed exceeds 2.7–3.6 times the root-mean-square horizontal velocity fluctuation.

I. INTRODUCTION

For flow speeds not too small, the method by which to convert a spectrum of a turbulent variable from the frequency domain for measurements taken at a fixed point to the wavenumber domain is well known.[1] It is to use Taylor's "frozen turbulence" hypothesis,[2]

$$k = 2\pi/\lambda = 2\pi n/\bar{u}\,, \tag{1}$$

where k is the assumed wavenumber, λ is the assumed wavelength along the direction of the mean wind, n is the frequency (number of cycles per unit time) measured at the fixed point, and $\bar{u}$ is the mean wind speed at the height of measurement. Studies of the accuracy of (1) have usually focused upon estimating how large the turbulence intensity can become before the frozen turbulence hypothesis should be considered invalid.[1] The effect of mean wind shear upon the hypothesis has been treated by Lin[3] but it was shown by Lumley[4] that the effect of the fluctuating eddy-convection velocity is more important, at least for the higher frequencies.

Both Lumley[4] and Wyngaard and Clifford[5] theoretically studied the effect of turbulent intensity upon the hypothesis with respect to the validity of $\lambda = \bar{u}/n$ for the higher frequencies. They assumed that the higher wavenumber turbulence is transported in a frozen state by the mean flow plus low wavenumber eddies. Thus, they relaxed the assumption that it is transported in a frozen pattern by a constant mean flow. They found that the effect of the latter assumption is to spuriously enhance the spectral intensities in the inertial subrange and at other frozen-turbulence wavenumbers past the energy containing range, but that the amount of enhancement is negligible in many typical instances.

It is of interest to make direct spectral measurements to check the validity of the frozen turbulence hypothesis not only to test the existing theories, but also to examine how the low wavenumber portion of the spectrum is affected.

Direct checks on the hypothesis in the lower atmosphere would involve along wind flights of an instumented aircraft past a tower instrumented at the same height, and a subsequent comparison of spectra. The aircraft speed would be sufficiently great so that the longitudinal spectrum determined from its data would be considered free of temporal effects. Such checks would probably show that the frozen turbulence hypothesis as applied to the tower data is typically grossly correct. Definitive comparisons would be difficult, however, because observed differences of up to ±50% in various parts of the spectrum could be ascribed to different instrumental techniques, to inhomogeneous turbulence along the mean wind direction, to mesoscale variations in the mean wind itself, to a nonrepresentative location of the tower, and/or to sampling error.

Here, laboratory measurements of temperature spectra in a freely convecting mixed layer will be utilized in an attempt to overcome these difficulties. The mean wind is simulated by passing a sensor through the fluid at a known, steady velocity. In this way, the effective mean velocity can be varied without altering the turbulence structure, and it can be made sufficiently small so that obvious shortcomings of the frozen turbulence hypothesis for large turbulence intensities should become apparent. The laboratory free-convection mixed layer is believed to simulate not only truly free convection in the atmosphere (a rarity) but, above the surface layer, to simulate convective boundary layers in general with mean wind speeds of up to 5 msec^{-1} or possibly even 10 msec^{-1}. In the field experiments of Kaimal *et al.*,[6] for example, free-convection mixed-layer scaling appeared to be successful with winds this large.

Previously, laboratory measurements designed to test the frozen turbulence hypothesis were made by Fisher and Davies.[7] They studied the turbulent flow within the mixing region of a circular jet

 0031-9171/82/010021-08$1.90

where effects of mean shear were especially large, and did not examine the effect of the hypothesis upon the true spatial or longitudinal spectrum. However, their procedure of treating space- and auto-correlations in a reference frame moving with the speed of the mean flow will be utilized here.

II. EXPERIMENTAL PROCEDURES

A. The laboratory model

The spectral measurements were made in the penetrative convection tank described by Willis and Deardorff.[8] The working fluid is water. The convective turbulence is generated by heating the fluid layer from below, the lower boundary condition being one of essentially constant temperature in the horizontal. The turbulent variable to be investigated is the fluid temperature, T. The mean mixed-layer height, h, averaged 0.24 m while the side-wall separation was 1.2 m. Above the slowly growing mixed layer was a stable layer of constant stratification. These and other conditions of the experiments were as in experiment E6 of Deardorff *et al.*,[9] except that no large-scale subsidence was applied.

Temperatures were measured at the height $z = 0.10h$ with three thermocouples, each of effective diameter 0.08 mm and estimated time constant for $u = 4$ cm sec^{-1} of 0.002 sec. The thermocouples, separated laterally a distance of 0.15 m from each other, could be translated across the convection tank at any desired speed. A photograph of the convection tank with the thermocouple support frame in place is shown in Fig. 1. Since there is no mean flow in the tank, the translation speed, u_0, simulates a mean wind speed, $\bar{u}$. In the absence of mean wind shear effects, $\bar{u}$ serves merely to translate the mixed layer turbulence across the warm surface. At the height studied, relative to h, little or no wind shear is to be expected in an atmospheric mixed layer stirred by thermal convection[10] in the absence of strong baroclinity.

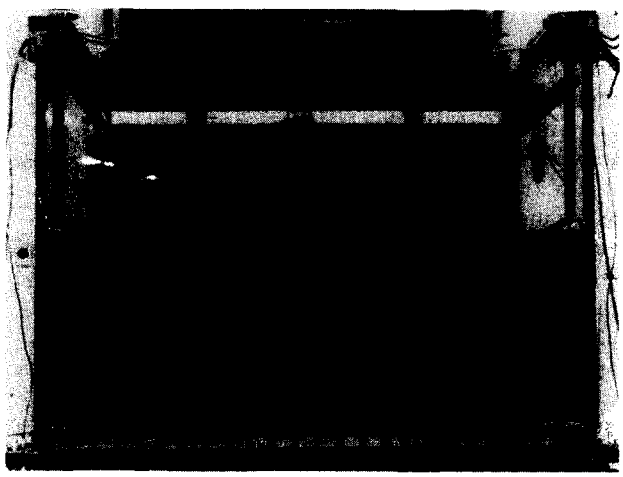

FIG. 1. Side-view photograph of the convection tank showing the three thermocouple support rods extending downwards. System can be translated at uniform speed in and out of the plane of the picture. Double horizontal line, occuring at a height of $1.8h$, is caused by reflection from upper surface of water. The thermocouple junctions and lead wires are of too small a diameter to show in the photo.

B. Experimental scale factors and parameters

Three thermocouple translation experiments (cases 1–3)were made with decreasing ratios u_0/w_*, where w_* is the mixed layer free-convection velocity scale

$$w_* = [g\alpha(\overline{W'T'})_s h]^{1/3}, \tag{2}$$

g is the gravitational acceleration, α is the thermal coefficient of expansion ($1/T$ in the atmosphere), and $(\overline{w'T'})_s$ is the vertical flux of temperature close to the surface. Another scale of interest, the temperature-fluctuation scale T_*, is defined by

$$T_* = (\overline{w'T'})_s / w_*. \tag{3}$$

Average values of these and other quantities during the experiments are listed in Table I. The rate of dissipation is estimated to have been 1 (mm)^2 sec^{-3}, and the Kolmogoroff microscale 1 mm at the height studied.

The heat flux $\overline{w'T'}_s$ in (2) and (3) was obtained from the approximate formula

$$\overline{w'T'}_s = h(\partial\bar{T}/\partial t)/1.25, \tag{4}$$

which was found to hold well, on the average, in Ref. 9. The mean mixed-layer height h was obtained from examination of the positional variations of a horizontally spread laser beam passing through the fluid at the height where index of refraction variations are maximal.

Each thermocouple signal was fed into a six-pole anti-aliasing filter with 3 dB point of 50 Hz.

There were nine experiments each involving three runs or transverses with the set of three thermocouples. The first and third run of an experiment used one value of u_0 while the second run used a different value. One of these values of u_0 was always about 4 cm sec^{-1}, corresponding to case 1 in Table I. This was the maximum translation speed utilized because preliminary studies indicated that excessive temperature fluctuations were generated near and above $z = h$ when a translation speed twice this large was utilized. Each run extended over a horizontal length of about 1m in cases 1–3 (see also Table I).

One additional set of experiments was conducted with $u_0 = 0$ (case 4). In that case, six sets of three spectra were obtained. The time period covered by each thermocouple traverse or time series, t_{max}, has been normalized by h/w_* and also presented in Table I.

Results from case 1 will be assumed to approximately depict the instantaneous temperature-fluctuation statistics along a horizontal line, with those from cases 2–4 being increasingly affected by temporal effects.

C. Data collection and analysis

The instantaneous, digitized data were recorded on magnetic tape at varying rates, always yielding the same number of data points, 2048, per run. That is,

TABLE I. Parameters of the experiments.

Case	u_0/w_*	No. of runs	No. of spectra	h(cm)	w_* (cm s^{-1})	T_* (C)	$(\overline{T'^2})^{1/2}$ (C)	x_{max}/h	$w_* t_{max}/h$
1	4.27	13	39	23.6	0.92	0.17	0.43	4.10	0.96
2	0.51	4	12	24.3	0.94	0.17	0.46	4.18	8.27
3	0.27	4	12	23.2	0.91	0.17	0.51	4.00	15.37
4	0.0	6	18	24.1	0.92	0.16	0.48	...	10.99

the time interval between successive data values was $t_{max}/2048$ (see Table I).

The mean and mean trend were removed from the data of each thermocouple transverse or time series, and also any mean curvature in cases 2–4. End sections of the records (5% at each end) were then tapered quadratically so that end points would be matched. The latter two procedures affected the temperature variance negligibly, whereas removing the mean trend decreased it very substantially in cases 2–4. Fast Fourier analyses were then performed, and individual spectral intensities $S_T(N)$ were normalized by the $\overline{T'^2}$ value occurring during each traverse before averaging individual spectra together. This procedure was followed because $(\overline{T'^2})^{1/2}$ and T_* decreased slowly during each experiment, by 24% on the average, as the water in the tank gradually warmed; values of w_* were essentially constant. In $S_T(N)$, N is the wave harmonic number ($N = 1, 2, 3 \ldots 1024$), with $N = 1$ representing the longest full wave present of period t_{max} or length x_{max} (see Table I), and $N = 1024$ representing the Nyquist frequency. The analysis described eliminated the $N = 0$ "wave."

In each experiment, statistics of the first and third runs were averaged together so that they would be directly comparable to those of the second (middle) run. Thus, sets of either three or six individual normalized spectra were first averaged together digitally; these averages were then further averaged together graphically, over several experiments, yielding an ensemble containing the total number of individual spectra per case as given in Table I, column 4. In addition, spectral values of $NS_T(N)/\overline{T'^2}$ were band averaged, for $n > 50$, over intevals of $\Delta N = 0.04\,N + 1$; for $2 \leq N \leq 50$ neighboring spectral values were averaged in trios with quarter–half–quarter weighting.

Mean spectra, $S_T(N)/\overline{T'^2}$ for the four cases were then transformed, using the same general type of fast-Fourier technique, to obtain the space–time correlation function $r(\delta x, \delta t)$, for separations δx, δt extending up to $\frac{1}{2}x_{max}$ and $\frac{1}{2}t_{max}$, respectively (and for $\delta x/\delta t = u_0$). As a check of the technique, it was noted that $r(0, 0) = 1$ and that the discrete, finite version of

$$\int_0^\infty r(x)dx = 0 \tag{5}$$

was obeyed. The latter result stems from the identity[2,11]

$$S_T(N)\overline{T'^2} = 4\int_0^\infty r(x)\cos 2\pi Nx\,dx \tag{6}$$

for $N = 0$ when $S(0) = 0$ and the individual data records can be considered periodic. Analogous expressions hold when time replaces the longitudinal x coordinate. Although identity (5) means that the Eulerian integral length and time scales are zero in this analysis, that result simply indicates that a different measure of integral scale is needed in turbulence studies, such as the length scale at which the correlation function first crosses zero. (The requirement that the Eulerian integral scale vanish guarantees that there will be a zero-crossing of the correlation function.) A more detailed discussion of this interpretation of (5) can be found in Ref. 12.

The standard deviation of the temperature fluctuations is also presented in Table I. Judging from these results, and also from the scatter in $\overline{T'^2}$ values between different experiments and between individual runs (1st plus 3rd versus the 2nd) of a given experiment, the variability appears attributable to sampling error. The existence of this much variability is another reason why individual spectra were normalized by the individual temperature variances. The average variance, 0.22 C^2, normalized by T_*^2, agrees with a free-convection surface-layer evaluation of Wyngaard *et al.*[13] to within 6% for $z/h = 0.10$.

III. LABORATORY RESULTS

A. Spectra

The normalized spectral intensities, $S_T(N)/\overline{T'^2}$, after multiplication by N, are shown on the log–log plot of Fig. 2 for the four cases. For cases 1–3 with translating thermocouples, the λ/h scale on the abscissa applies, where λ is the wavelength (frozen wavelength in cases 2 and 3). For case 4 only ($u_0 = 0$) the $\tau w_*/h$ scale applies instead, where τ is the period. In all cases the N scale applies. The ordinate can be considered to be as shown, or to be $nS_T(N)/\overline{T'^2}$ or $kS_T(k)/\overline{T'^2}$ as appropriate. Here, the sensor translation speed, u_0, in the absence of a mean wind is identified with a mean wind, $\bar{u}$, for a fixed-point measurement in the atmosphere under conditions when $-z/L$ exceeds 1 to 10, where L is the Monin–Obukhov length.

The spectrum for case 1 exhibits a broad maximum centered in the vicinity of $\lambda = 0.15$ h. There is no inertial subrange because the molecular smoothing subrange ($\lambda/h < 0.03$) lies too close to the energy containing range. We notice, however, that for $z/h = 0.1$ Kaimal *et al.*[6] found the maximum in $NS_T(N)$ in the convecting boundary layer to be centered at the greater value of $\lambda = 1.2$ h. The discrepancy may be associated with the occurrence of significant horizontal variations in ground temperature over large scales at this or any

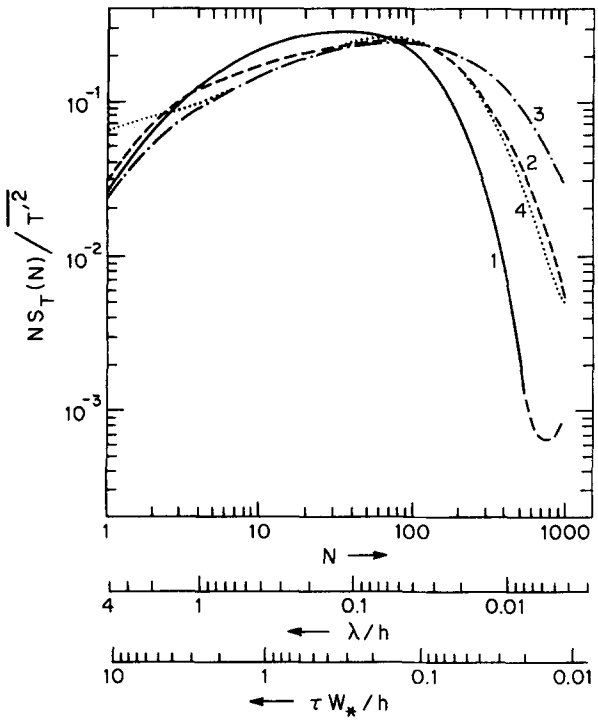

FIG. 2. Log–log plot of spectral estimates $NS_T(N)/\overline{T'^2}$. On abscissae, N is wave harmonic number, λ is a frozen-turbulence wavelength (cases 1–3) and τ is wave period (case 4 only).

other field site on sunny days. There is also the possibility that our power spectra exhibit the -1 subrange[14] associated with large Prandtl number ($Pr \cong 7$ in water), and that because of the absence of an extended inertial subrange, the -1 subrange [here a zero slope for the $NS_T(N)$ plot] appears as an extension to the right of the peak of the energy-containing range. Without high quality velocity spectra to accompany the temperature spectra, however, this latter interpretation remains uncertain. In comparing the effects of the frozen turbulence hypothesis on the laboratory temperature spectra with those to be expected for the lower atmosphere, we are therefore constrained to compare only broad spectral ranges, such as the main energy-containing range and the "high-wavenumber" range where N exceeds the value at which the true spatial power spectrum first exhibits the $-\frac{5}{3}$ slope.

For $\lambda/h < 0.008$ the case-1 spectrum contains noise believed to be associated partly with vibrations of the thermocouple support rods, partly with stray electrical voltages at frequencies aliased back into our observed spectrum, and partly with the limited resolution of the analog-to-digital data conversion system. However, this noise level is sufficiently low, and at sufficiently high frequencies in time, so that its presence is not even detectable in cases 2–4.

The spectra of cases 2 and 3 exhibit systematic enhancement at the higher wavenumbers when λ is obtained from (1) using the frozen turbulence hypothesis in qualitative agreement with theory.[4,5] It is seen that the added intensity at high wavenumbers has been borrowed from an extensive region of the energy-containing range out to rather small wavenumbers. This has caused the maximum of $NS_T(N)$ to shift from $\lambda = 0.15$ h to about 0.05 h. The longest frozen-turbulence waves of scale comparable to 2 h and greater are apparently unaffected by the frozen-turbulence hypothesis for simulated wind speeds as small as we could utilize (case 3). The net effect is an overall broadening of the apparent spectrum.

The temporal spectrum for case 4 of Fig. 2 cannot be compared very closely with those of cases 1–3 since its position on the plot depends on the arbitrary placement of the time scale on the abscissa relative to the space scale.

B. Space- and auto-correlations

The correlation functions $r(\delta x, \delta t)$ are shown in Fig. 3 on a semilog plot so that values for both small lag (except zero) and large may be examined. (The spatial scale on the abscissa, $\delta x/h$, applies to all but the temporal case while the different temporal scales are as designated for cases 1–3. For case 4 the uppermost labeled abscissa applies.) It was found that the r curves shown, being derived from smoothed spectra, are very smooth whereas those which could be derived from individual spectra, and subsequently averaged, contained much statistical uncertainty reflected in irregularities. The r curves of Fig. 3 and the spectra of Fig. 2 contain equivalent information about the temperature fluctuations, since one may be derived from the other.

The enhanced spectral intensity at the higher wavenumbers as u_0/w_* becomes small in Fig. 2 is now seen to be associated with the more rapid loss of correlation at small lags in cases 2 and 3 than in case 1.

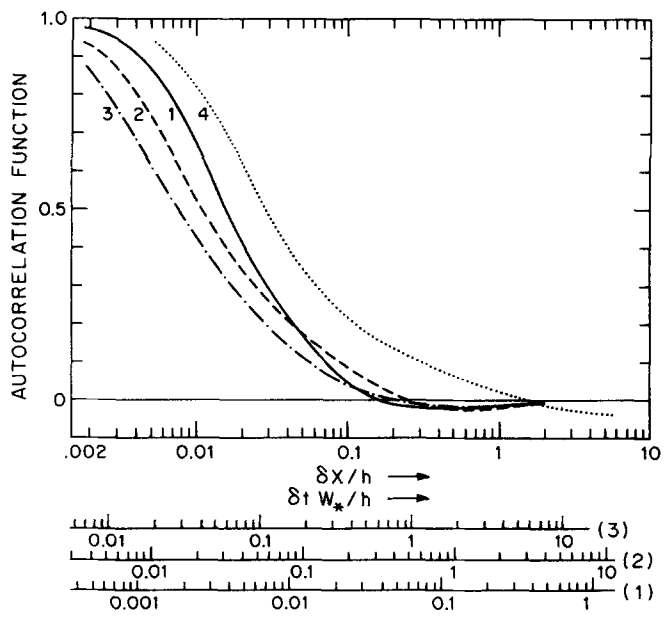

FIG. 3. Autocorrelations of temperature fluctuations sensed by the moving sensors (cases 1–3) and the stationary sensors (case 4), as a function of normalized spatial separation $\delta x/h$ in cases 1–3 or of normalized time lag (cases 1–4). Uppermost labeled abscissa applied to both $\delta x/h$ for case 1 and the time lag for case 4. Other abscissae apply to case 1, 2, or 3 as designated.

The lag in x at which r crosses zero happens to coincide closely with the λ/h value of maximum $NS_T(N)$ for case 1. However, for cases 2 and 3 this is not true. The zero-crossover lag scale exceeds the $1/e$ lag scale by factors of 7, 14, 19, and 34 for cases 1–4, respectively. The zero-crossover length scale from case 1 is seen to be equal to about $0.1\,w_*$ of the zero-crossover time-lag scale from case 4.

IV. SPACE-TIME CORRELATION DIAGRAM

It is of interest to plot the space-autocorrelation function in the manner suggested by Ref. 7 for which, after using mixed-layer scaling, the ordinate becomes

$$\delta x' = \delta x/h - (u/w_*)\delta t' , \tag{7}$$

and the abscissa is

$$\delta t' = (w_*/h)\delta t . \tag{8}$$

Then, if the turbulence pattern itself is independent of the mean flow speed (and dependent only on z, h, w_*, ...) the correlation diagram will have a unique appearance independent of the mean flow. This has been done for the present data for very small lags in Fig. 4 and for larger lags in Fig. 5. In our case $\bar{u}=0$ in (7), and a data-collection path is determined simply by a slant ray in the diagram of slope

$$\delta x'/\delta t' = (\delta x/\delta t)/w_* = u_0/w_* . \tag{9}$$

That is, as a thermocouple passed through the field of temperature fluctuations at speed u_0 relative to any mean flow, a spatial lag, δx, was always related to a lag in time, δt, by the relation $\delta x/\delta t = u_0$. Hence, from (9), the data lay along the slant ray in Fig. 4 or 5 having the particular value of u_0/w_* employed in that experiment. The data available for constructing these diagrams thus lay along only the three slant rays shown, and the abscissa. Hence, considerable uncertainty must be admitted to exist in the interpolated regions, particularly to the right of the $u_0/w_* = 0.27$ ray.

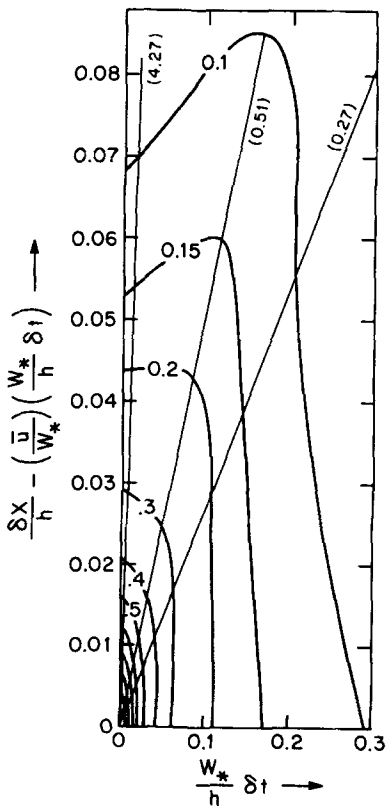

FIG. 4. Orthogonal representation of the correlation function, r (contours labeled) on the universal diagram, for small spatial time separations.

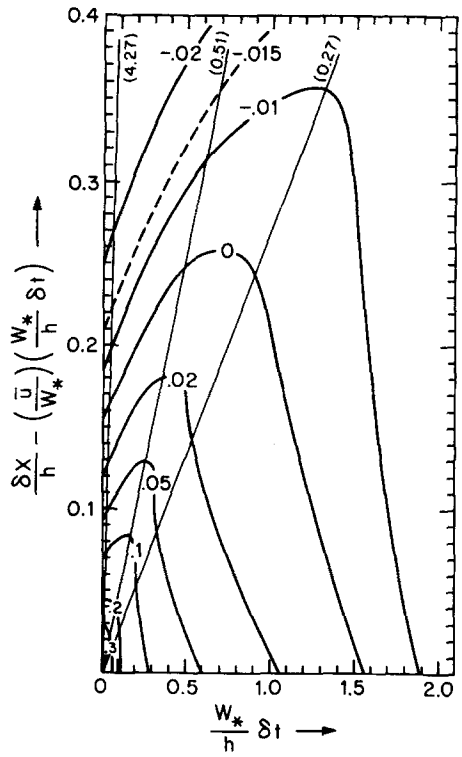

FIG. 5. Contours of the correlation function, r, on the universal diagram for intermediate spatial and time lags.

If a mean flow $\bar{u}$ had existed, the meaning of a slant ray in the universal correlation diagram would be the same as when there was no mean flow and a single sensor traveled at speed $u_0 = \bar{u}$. That is, the slope of the ray is then determined from (7), (8), and (9) to be $(\delta x/\delta t - \bar{u})/w_* = u_0/w_*$. For a single sensor fixed to the surface, $u_0 = -\bar{u}$ and hence $\delta x = 0$; i.e., only changes in time are sensed. In that case, the slope of the ray on the universal correlation diagram is $-\bar{u}/w_*$. Owing to the fact that the correlation is an even function of $\delta x'$, however, its pattern in the 4th quadrant of such a diagram is the mirror image of the one in the quadrant shown. Thus, the data-collection ray for the fixed sensor in the mean flow can be considered to have the slope $+\bar{u}/w_*$ also. This demonstrates that the statistics collected from a sensor traveling at speed u_0 in the absence of a mean flow lie along the same ray in the universal diagram as would that measured at a fixed point in the presence of a mean flow of magnitude u_0 (provided mean shear effects do not extend up to the height of measurement).

In Figs. 4 and 5 the abscissa is scaled relative to the ordinate such that the $r=0$ contour crosses each coordinate axis at equal distances from the origin (see Fig. 5). If the temperature structure were isotropic with

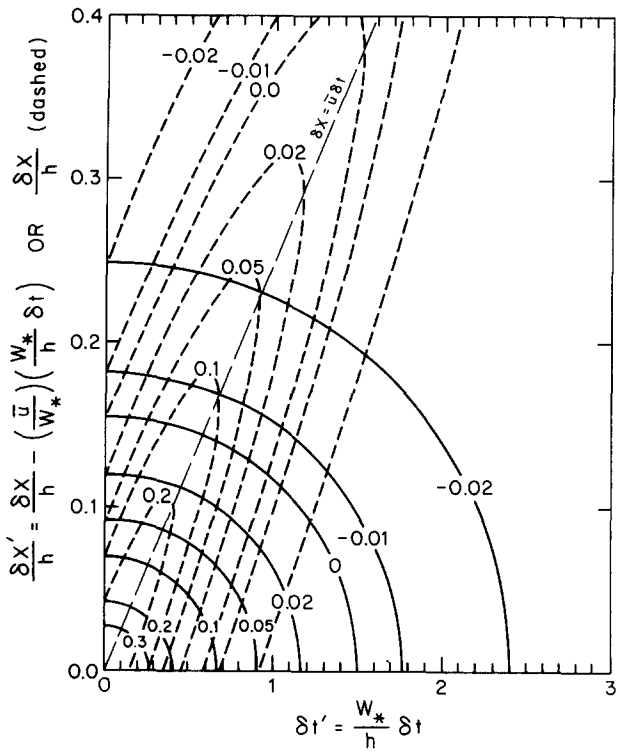

FIG. 6. Contours of the correlation function (solid arcs) for hypothetical turbulence that is isotropic in space–time separations; as ordinate use $\delta x/h - (\bar{u}/w^*)\delta t'$. Dashed ellipses are contours which would then occur if a mean flow $\bar{u} = 0.25w_*$ were present but the ordinate $\delta x/h$ is used. The long-dashed line is the data-collection ray in such a mean flow for a single sensor fixed relative to the surface.

respect to space and time, the contours would therefore be circular arcs as in Fig. 6 (solid curves). That is, r would be independent of the angle of a data-collection ray, and would depend only on the quantity $(\delta x')^2 + (L_x/L_t)^2(\delta t')^2$, where L_x is the dimensionless cross-over scale along $\delta x'$ where $r(\delta x', 0) = 0$, and L_t is the dimensionless cross-over scale along $\delta t'$ where $r(0, \delta t') = 0$. However, from Figs. 4 and 5, $r(\delta x', \delta t')$ is seen to be far from isotropic in space–time. At small values of $\delta x'$, the correlation drops off rapidly as $\delta t'$ increases while holding $\delta x'$ constant. At somewhat greater lags, on the other hand, a pronounced bulge of higher correlation develops in the vicinity of the $u_0/w_* = 0.51$ ray, and gradually shifts to the vicinity of the $u_0/w_* = 0.27$ ray for lags beyond which r has fallen to zero. Such anomalous structure in space–time was entirely unexpected, and no convincing explanation can be offered here. Yet, the spectra of Fig. 2 which yielded these space–time correlations appear to behave reasonably.

It may be pointed out that if the frozen turbulence hypothesis were strictly valid, the r contours of Figs. 4 and 5 would be horizontal lines intercepting the ordinate where the actual contours do. The universal diagram therefore emphasizes the lack of validity of the hypothesis for rays inclined appreciably from the vertical.

The diagram of Figs. 4 and 5 should not be confused with that for which a mean flow exists but for which the spatial-displacement coordinate does not have the $\bar{u}$ effect removed; e.g., see Ref. 1 (p. 194). Such a diagram applies only to the particular flow speed which occurred, although it may be converted into the universal diagram. For example, the hypothetical, isotropic space–time correlation pattern of Fig. 6 (solid curves) has been converted to the pattern (dashed curves) which would result had a mean flow $\bar{u} = 0.25w_*$ been present and the ordinate $\delta x/h$ utilized (translation effect not removed). The circular arcs then convert into highly elongated ellipses. Interestingly, their major axis is rotated counterclockwise slightly from the $\delta x = \bar{u}\delta t$ axis, which passes through the ellipses at the points where $\partial r(\delta x, \delta t)/\partial(\delta x) = 0$. For this reason, the value of $\delta x/\delta t$ at points where the latter criterion is fulfilled has been suggested as a definition of the eddy-translation speed.[7]

The elongation of the ellipses in Fig. 6 for $\bar{u} = 0.25w_*$ bears a partial resemblance to the bulge of high correlation in Fig. 5. Therefore, an explanation of the bulge might somehow involve the local translation of small thermal plumes carried by random larger scale horizontal convection currents having a magnitude of a few tenths of w_*. At the height in question, the total root-mean-square horizontal velocity component is about $0.5w_*$.[8] Another characteristic of the turbulence which may be involved in any explanation is the skewness of the temperature fluctuations. Small negative temperature deviations are very common while positive fluctuations are less frequent but much larger in magnitude.

In order to examine the space–time correlations on a $\delta x'$-$\delta t'$ plot out to much greater lags, the log–log plot of Fig. 7 has been constructed. In it, the slant rays of Figs. 4 and 5 are replaced by lines of unit slope. (The

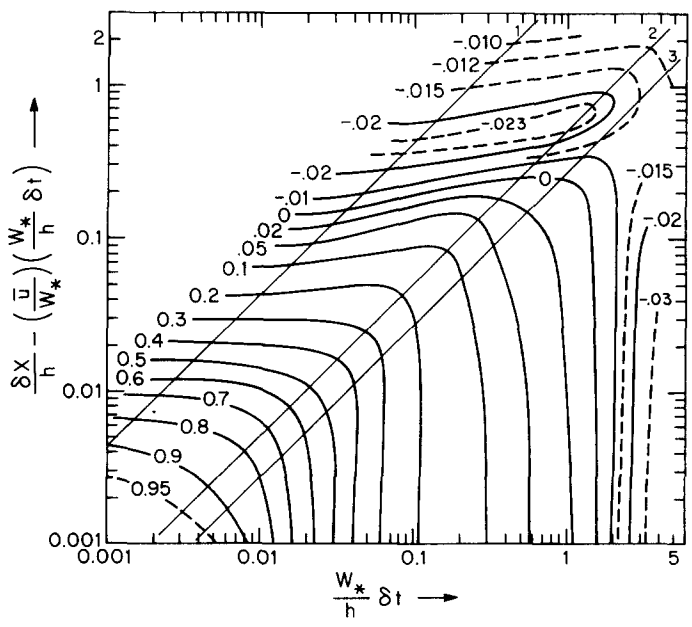

FIG. 7. Contours of the correlation function derived from cases 1–4 as a function of $\delta x'$ and $\delta t'$ using log–log coordinates. The data-collection rays for cases 1–3 are labelled at upper right. Data from case 4 were utilized in estimating r values along the abscissa.

associated u_0/w_* values are equal to the ordinate value where the unit-slope line intercepts the unit abscissa.) On this plot the most conspicuous feature is the split in the (negative) minimum lobe of r for large values of $\delta x'$ and $\delta t'$.

V. THE HYPOTHETICAL SPECTRUM VERSUS THE TRUE SPECTRUM ALONG x

The extent to which the frozen-turbulence hypothesis is valid, so that a spectrum measured at a fixed point in a mean flow closely yields the true spectrum along x, depends of course on how steep the slope of the $\bar{u}/w_*$ ray is in Fig. 4 or 5. The required magnitude of $\bar{u}/w_*$ depends on the purpose to which the spectrum is to be used as well as the particular pattern of the correlation contours associated with the particular turbulence in question. Since with the present free-convection turbulence w_* is a measure of $(\overline{u'^2})^{1/2}$, the validity of the frozen-turbulence hypothesis requires a small turbulence intensity, $(\overline{u'^2})^{1/2}/\bar{u}$, as has been pointed out in numerous previous studies.[1]

In the present study, the ability of data along the ray $u_0/w_* = 4.27$ to represent the true spectrum along x can be tested by estimating r along the $\delta x'$ axis ($\delta t' = 0$) by extrapolation. This procedure was followed, and extrapolated values of $r(\delta x', 0)$ obtained from Figs. 4–6 were then fast-Fourier transformed back into the spectrum. Since little extrapolation was involved, the resulting spectrum turned out to be virtually indistinguishable from that of case 1, Fig. 2, for $N < 200$, thus indicating the validity of the assumption made earlier that the spectrum for this case essentially represents the true spectrum along x. However, for $N > 200$ the spectrum reconstructed from the correlation function suffered oscillations about the case-1 spectrum which increased in amplitude as N increased, and which even led to negative spectral estimates in some high-wavenumber regions. Thus, small irregularities in $r(\delta x')$ can lead to relatively large oscillations in $S(N)$ at large N, while the transformation of $S(N)$ to yield $r(\delta x')$ provides a very smooth representation of the latter even if small irregularities in $NS(N)$ are present on the log–log plot.

In order to estimate how the spectra for $\bar{u}/w_* = 2$ and 1 would appear using the frozen turbulence hypothesis, values of $r(\delta x')$ were obtained along these two slant rays by interpolation from Fig. 7, and similar transformation to spectra while ignoring the fact that $\delta t'$ was not zero. The resulting spectra are shown in Fig. 8, along with those measured directly for cases 1–3. The forementioned difficulty associated with this procedure is evident for $N > 200$. However, for smaller N the spectra obtained from the interpolated correlation function behave in the expected sense. They suggest that, for most purposes, the criterion $\bar{u}/w_* > 1.5$ to 2 needs to be fulfilled in order that fixed-point spectra as a function of frequency, measured in the lower part of the convectively mixed layer in the atmosphere, satisfactorily represent the true spectrum as a function of a horizontal wavenumber along x.

If the universal correlation diagram had disclosed that the r pattern were approximately isotropic in space-time, a simple theory could have been constructed for the detailed behavior of the measured spectrum under the frozen-turbulence hypothesis. Along a ray corresponding to a particular value of $\bar{u}/w_*$, the projection of any particular r = const value from along an arc of Fig. 6 horizontally onto the $\delta x'$ axis would yield a δx value that is smaller than the true δx value for that r by the factor

$$F = [1 + (L_x/L_t)^2(\bar{u}/w_*)^2]^{-1/2}. \tag{10}$$

The same factor would apply anywhere along the same ray. From relation (6) it can then be shown that this apparent contraction of δx would lead to an apparent stretching of the spectral wavenumber, or of N, by the same factor. On a log-log plot, this stretching would appear as a simple shift of the entire $NS(N)$ spectrum to the right. From Fig. 2 we see that such a shift to the right does occur at the high wavenumbers but not at low wavenumbers, due to the space–time anisotropy of the temperature fluctuation field.

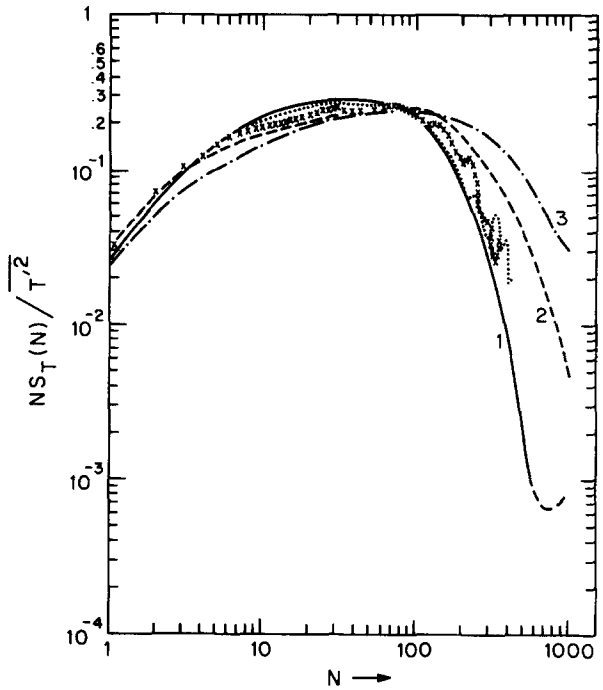

FIG. 8. Log–log plot of $NS_T(N)$ versus N for spectra derived from interpolation of the correlation function along the $\bar{u}/w_* = 2$ ray (dots) and along the 1 ray (crosses). Measured spectra for cases 1–3 are also shown.

VI. SUMMARY

An investigation of the frozen-turbulence hypothesis for free convection in the laboratory, at a small height within the turbulent layer, indicates that the temperature spectrum is shifted toward larger k at high wavenumbers but is not shifted at low wavenumbers. The extra spectral intensity at higher wavenumbers is borrowed from the energy containing region over a broad band of wavenumbers. Although the results are in qualitative agreement with theory,[4,5] no quantitative comparison is made because of the absence of any extended inertial subrange in the laboratory mixed layer.

The space–time correlation function is examined on the universal diagram suggested by Fisher and Davies.[7] It is found to be highly anisotropic, which explains why the effect of the frozen turbulence hypothesis is not simply to shift the spectrum to the right at all wavenumbers, on a log–log plot.

An interesting peculiarity of the measured space–time correlation pattern, on the universal diagram, is a bulge of higher correlation extending along a ray corresponding to small time lags but moderate spatial separations. This anomaly is unexplained.

Based on interpolated space-autocorrelation functions, spectra obtained by the frozen turbulence hypothesis appear to be satisfactory representations of the true temperature spectrum along x, for the mixed-layer conditions treated, if $\bar{u}/w_*$ exceeds 1.5 to 2. This converts to the criterion that $\bar{u}/(\overline{u'^2})^{1/2}$ should exceed a value in the range 2.7–3.6.

The conventional Eulerian integral length scale, or time scale, is shown to be no measure of the dominant eddy scale. Instead, it is zero[12] when the data are preconditioned to have zero mean before individual spectra are obtained. The scale at which the correlation function crosses zero was instead used as an appropriate length or time scale for the dominant eddies represented by the data. The ratio of the horizontal separation scale at zero-crossover to the time-lag scale at its crossover point was found to be about $0.1\ w_*$ for the temperature measurements made at a height of 0.1 h.

In this study it has been assumed that the turbulence structure of the thermal convection is independent of any mean flow that may be present. Outside of a laboratory tank this assumption is only true for measurement heights substantially in excess of the (negative) Monin–Obukhov length scale.

ACKNOWLEDGMENTS

We appreciate encouragement received from J. Wyngaard and helpful suggestions from C. Paulson at an early stage of this study. The technical assistance supplied by P. Stockton was indispensible. The software for obtaining numerically either the spectra or the autocorrelations by the fast-Fourier technique was developed by S. Yoon. Calculations were performed on Oregon State University's CYBER computer.

This study was supported by the Atmospheric Research Section of the National Science Foundation under Grant No. ATM 77-24507.

[1]J. L. Lumley and H. A. Panofsky, *The Structure of Atmospheric Turbulence* (Interscience, New York, 1964).
[2]G. I. Taylor, Proc. R. Soc. London Ser. A **164**, 476 (1938).
[3]C. C. Lin, Appl. Math. **10**, 295 (1953).
[4]J. L. Lumley, Phys. Fluids **8**, 1056 (1965).
[5]J. C. Wyngaard and S. F. Clifford, J. Atmos. Sci. **34**, 922 (1977).
[6]J. C. Kaimal, J. C. Wyngaard, D. A. Haugen, O. R. Coté, Y. Izumi, S. J. Caughey, and C. J. Readings, J. Atmos. Sci. **33**, 2152 (1976).
[7]M. J. Fisher and P. O. A. L. Davies, J. Fluid Mech. **18**, 97 (1964).
[8]G. E. Willis and J. W. Deardorff, J. Atmos. Sci. **31**, 1297 (1974).
[9]J. W. Deardorff, G. E. Willis, and B. H. Stockton, J. Fluid Mech. **100**, 41 (1980).
[10]S. P. S. Arya and J. C. Wyngaard, J. Atmos. Sci. **32**, 767 (1975).
[11]F. Pasquill, *Atmospheric Diffusion* (van Nostrand, London, 1962), p. 3.
[12]G. Comte-Bellot and S. Corrsin, J. Fluid Mech. **48**, 273 (1971).
[13]J. C. Wyngaard, O. R. Coté, and Y. Izumi, J. Atmos. Sci. **28**, 1171 (1971).
[14]G. K. Batchelor, J. Fluid Mech. **5**, 113 (1959).